Journal of Research and Applications in Mechanical Engineering
ISSN: 2229-2152 (Print); 2697-424x (Online)
(2025) Vol. 13, No. 2, Paper No. JRAME 25-13-021
[DOI: 10.14456/jrame.2025.21]

Research Article

Nonlinear Vibration Analysis of Phased-controlled Actuator Capable of Movement inside Iron Structures

H. Yaguchi*
R. Sato
Faculty of Engineering, Tohoku Gakuin University, Itsutsubashi Campus, 984-8588, Japan

Received 2 August 2024
Revised 23 October 2024
Accepted 27 October 2024

Abstract:
In recent years, an iron structures that form the framework of buildings, bridges, and other structures have become enormous. As a result, workers are performing hazardous work such as welding and cutting at high altitudes. Due to a falling birth rate and aging population, Japan has a shortage of workers in various fields. Automation using robots is thus promoted at in various fields. In this study, a phase-controlled actuator is proposed as a power source for robots. A two-degree-of-freedom nonlinear vibration model of the actuator is theoretically analyzed. A static analysis of the actuator movement is also carried out. It is found that the movement characteristics of the actuator can be predicted based on the theoretical analysis results. Furthermore, it is verified that the results of the theoretical analysis well agree with the measurement results obtained in device tests. A single phase-controlled actuator can play the role of several motors. Furthermore, if this phase-controlled actuator is equipped with a micro camera, visual inspection of iron structures can be performed.

Keywords: *Vibration analysis, Nonlinear, Actuator, Phase-controlled*

1. Introduction

In recent years, an iron structures that form the framework of buildings, bridges, and other structures have become enormous. As a result, workers are performing dangerous tasks such as welding and cutting at high altitudes. Due to a falling birth rate and aging population, Japan has a shortage of workers in various fields. For this reason, labor shortages at construction sites have become a major social problem. Automation using robots is thus promoted. Material transfer robots [1], rebar tying robots [2], and welding robots [3] have been proposed to address the worker shortage at construction sites. However, few practical examples have been demonstrated and complex tasks are difficult to automate. The automation of construction using robots is an important priority for ensuring worker safety and improving work efficiency. In such a robot, at least two electromagnetic motors are required as a power source to move such a robot. Generally, in robots equipped with large electromagnetic motors with good torque characteristics, movement in the vertical plane is markedly degraded in performance due to the self-weight of these motors. When a small electromagnetic motor is used to design a compact drive unit, movement in the vertical plane is expected to have poor performance due to insufficient torque.

On the other hand, ultrasonic motors exist as a counterpart to electromagnetic motors. Ultrasonic motors are a typical example of phase-controlled actuators using multiple vibration elements. These can be divided into two types: standing wave [4] and progression wave [5-7]. These motors are driven by the elliptical motion of multiple piezoelectric elements, with the phase difference between the vibrations of the piezoelectric elements set at 90 degrees to achieve rotational or linear motion. The operating principle and design method of this motor have been almost completely established.

* Corresponding author: H. Yaguchi
E-mail address: yaguchi@mail.tohoku-gakuin.ac.jp

Ultrasonic motors produce high torque at low speeds and are often used in the drive section of a robot. However, ultrasonic motors require a dedicated controller, are less durable and are quite expensive. Furthermore, in electromagnetic motors, a method to improve torque characteristics has been established using phase control of input voltage [8, 9]. There are many examples of phase control in electric circuits. On the other hand, no research examples can be found for phase-controlled actuators that combine electromagnetic force with mechanical vibration and are capable of linear and rotational motion.

Based on these, the authors previously proposed the operation principle of a phase-controlled actuator [10, 11], in which multiple vibration components are orthogonally arranged and the phase of the vibration is used to enable movement inside iron structure. The actuator is attached to the magnetic material using the attractive force of a permanent magnet, allowing it to move freely within iron structure. The vibration amplitude of the actuator was measured during movement, and a static analysis was performed to predict the movement characteristics of the actuator using this vibration amplitude. The results of the analysis agreed well with the experimental results, demonstrating the validity of the theoretical analysis. Tests on actual equipment have shown that this actuator has high propulsive performance and good controllability. To make the actuator lightweight and compact, an electromagnet is inserted into the vibration component that serves as the propulsion source. Therefore, the vibration component exhibits nonlinear behavior. However, the vibration amplitude cannot be calculated theoretically because the dynamic analysis of the actuator has not yet been performed. For the nonlinear problem of a one-degree-of-freedom model, a number of analysis methods have been proposed. In contrast, the harmonic balance [12] method and the average method [13] have been proposed as methods for analyzing nonlinear models with multiple degrees of freedom, but these methods are complicated to analyze and have not yet been established as the definitive analysis method. Therefore, with the development of analytical software, methods using numerical simulation have become the mainstream [14, 15]. However, in the case of simulation-based calculations, the model is completely specific and cannot be applied to a wide range of problems. Theoretical analysis is important in engineering to systematically clarify nonlinear behavior. Therefore, it is desirable to carry out a theoretical nonlinear vibration analysis, and predict the movement characteristics of actuators.

Furthermore, the translational and rotational movements of the phase-controlled actuator [10, 11] treated in the previous study were restricted to a single drive. In this paper, a new phase-controlled actuator is proposed that is capable of both translational and rotational movement. A two-degree-of-freedom vibration model of the phase-controlled actuator, where the nonlinearity of the coil spring is linearized using an equivalent linearization method, is theoretically analyzed. A static analysis of the actuator was also performed, incorporating new effects of load mass and traction force. By combining static and dynamic analysis, it was shown that the movement characteristics of the actuator can be numerically predicted. In addition, a prototype of the actual phase-controlled actuator was built and tested. The results of the theoretical analysis well agree with the measurement results obtained in device tests, verifying the validity of the theoretical analysis. It is shown that the movement characteristics of the actuator can be predicted based on the theoretical analysis results.

This actuator is lightweight and simple in design and can be directly driven. The control of the vibration phase difference in a vibration component enables translational and rotational reciprocating movement, allowing a single actuator to play the role of several motors. The operation principle of the actuator, which can be applied as a drive source for material transfer and work robots inside iron structures, is established here. Furthermore, if this phase-controlled actuator is equipped with a micro camera, visual inspection of iron structures such as cable-stayed bridges can be performed.

2. Structure of phase-controlled actuator

Figure 1 shows a phase-controlled actuator capable of reciprocating movement (translational and rotational) on a magnetic material. The actuator consists of three vibration components (A, B and C) with identical dimensions, an acrylic frame, an acrylic plate and three acrylic rods attached to the bottom of the frame, an NdFeB permanent magnet, and a natural rubber sheet. The main permanent magnet (mounted in the center) was fitted to hold the actuator to the magnetic material. Two secondary-permanent magnets were mounted at r = 22.5 mm from the center of the actuator to ensure stable translational movement of the actuator. The main permanent magnet has a diameter D of 10 mm and a thickness of 2 mm. Each secondary-permanent magnet has a diameter d of 6 mm and a thickness of 1 mm. The natural rubber sheet, which has a thickness of h = 1 mm, was glued to the bottom of the three permanent magnets to increase the frictional force.

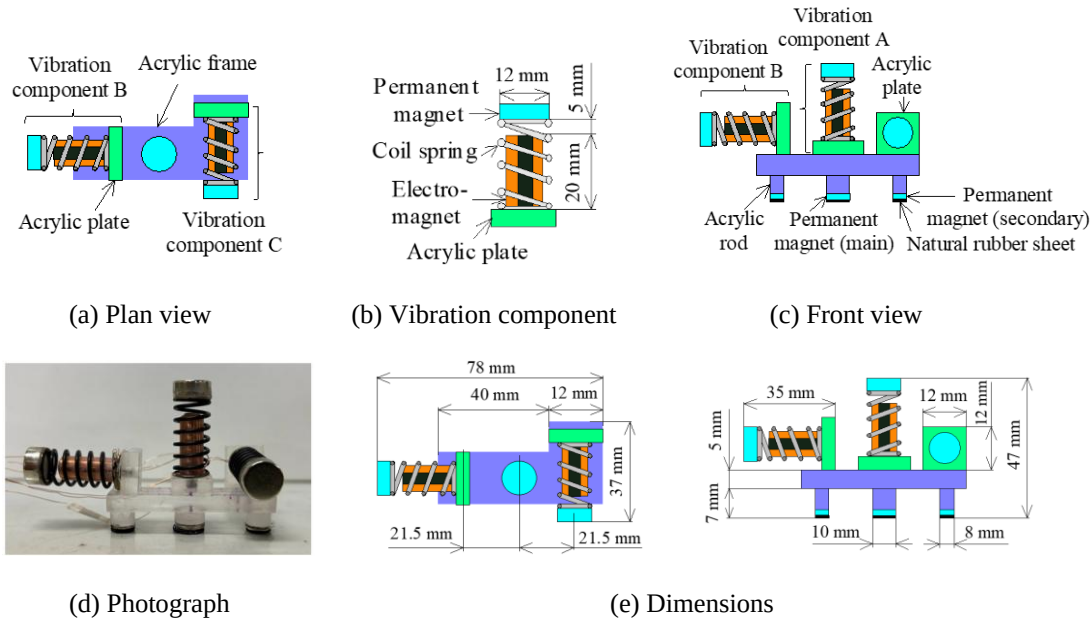

(a) Plan view (b) Vibration component (c) Front view

(d) Photograph (e) Dimensions

Fig. 1. Structure of phase-controlled actuator.

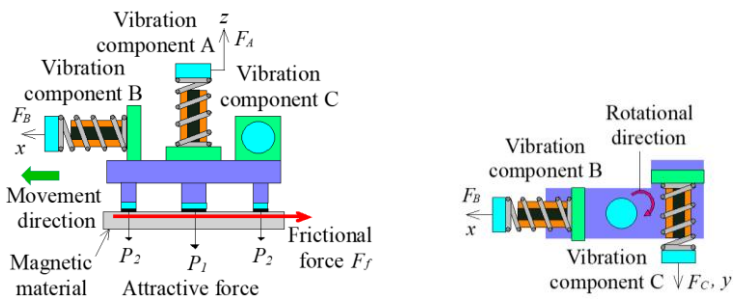

(a) Translational movement (b) Rotational movement

Fig. 2. Operation principle of phase-controlled actuator.

Vibration component A was mounted at the center of the frame. Vibration components B and C were positioned orthogonally to component A and mounted on opposite sides at R = 21.5 mm from the center. The coil springs acting as the vibration components are made of stainless steel and have an outer diameter of 12 mm and a free length of 25 mm The NdFeB permanent magnet is 12 mm in diameter and 5 mm in height. It is magnetized in the height direction. The electromagnet consists of a 3.8-mm-diameter iron core wound 840 times with 0.2-mm-diameter copper wire. The gap between the iron core and the permanent magnet is 5 mm when stationary. The dimensions of the actuator are 47 mm (height), 78 mm (length), and 37 mm (width). The total actuator mass m is 56.3 g.

For vibration components A, B and C, the displacement coordinates x, y and z are defined as shown in Figure 2 to illustrate the operation principle of the actuator. When the actuator is set on the magnetic material, the attraction force due to the main permanent magnet is P_1 and the attraction force due to the secondary-permanent magnet is P_2.

As shown in Figure 2(a), if vibration component A is displaced with amplitude B_{be} in the $+z$ direction, the friction force F_f decreases due to the generated force F_A. When component B is displaced with amplitude B_{bs} in the $+x$ direction, the actuator tends to slide in the $+x$ direction due to the generated force F_B. When the permanent magnet of vibration component A is displaced with amplitude B_{be} in the $-z$ direction, the friction force F_f increases due to the generated force F_A, and even if component B is displaced with amplitude B_{bs} in the $-x$ direction, the movement in the $-x$ direction is small. The actuator therefore moves in the $+x$ direction.

On the other hand, as shown in Figure 2(b), when vibration component A is displaced with amplitude B_{be} in the $+z$ direction, the friction force F_f decreases. When vibration component C is displaced with amplitude B_{br} in the $+y$ direction, a moment acts on the frame center due to the generated force F_C and the actuator tends to rotate clockwise. If vibration component A is displaced with amplitude B_{be} in the $-z$ direction, the actuator is less likely to rotate counter-clockwise when component C is displaced with amplitude B_{br} in the $-y$ direction due to the increased frictional force F_f. The direction of translational and rotational movement of the actuator can be controlled by operating the two vibration components at the same frequency and setting the phase difference of the vibrations between the components to 0 (in phase) or 180 (out of phase) degrees.

Vibration component of this actuator consists of the electromagnet inserted into the coil spring for the purpose of compact design. Due to the attraction force between the permanent magnet and the iron core of the electromagnet, the coil spring exhibits the behavior of a soft spring. The results of displacement measurements made with a force gauge and an x-y stage, when compressive and tensile forces are applied to the spring, show that the spring exhibits soft spring characteristics.

$$F(x) = k_2 x - \lambda x^3 = 1836\ x - 28.46\ x^3 \tag{1}$$

In equation (1), the units of force F, linear spring constant k_2, displacement x and coefficient λ on nonlinearity are are [N], [N/m], [m] and [N/m^3], respectively. Due to the relatively small nonlinearity of the coil spring, only third-order terms were considered as nonlinear terms in this study, as shown in a previous study [16].

3. Vibration analysis for translational movement

The case of two vibration components (A and B) operating is considered. The phase-controlled actuator shown in Figure 1 was modeled as a two-degree-of-freedom model, as shown in Figure 3. In this actuator, the attraction force of the actuator is much larger than the mass m_2 (0.0043 kg = 0.042 N) of each vibration component. Therefore, in the vibration analysis, the rubber sheet of the actuator was considered to be close to a fixed state, and the vibration analysis was performed. When vibration component A vibrates, as shown in Figure 3(a), the rubber sheet of the support part undergoes compression-tension deformation. On the other hand, when vibration component B vibrates, as shown in Figure 3(b), the rubber sheet undergoes shear deformation.

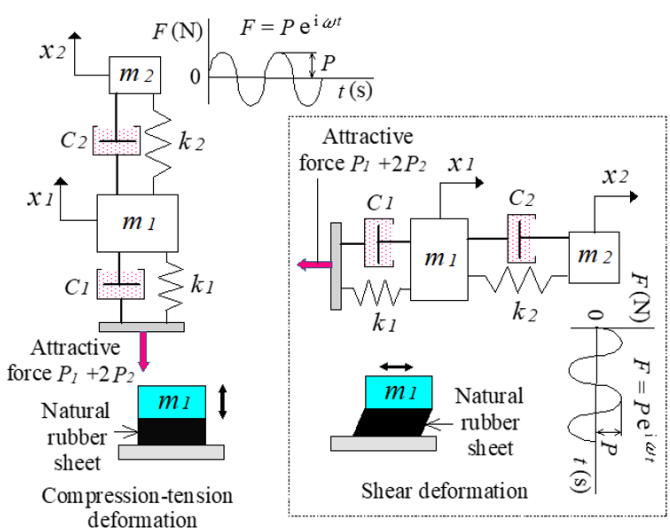

(a) Compression-tension model (b) Shear model

Fig. 3. Modeling of translational movement.

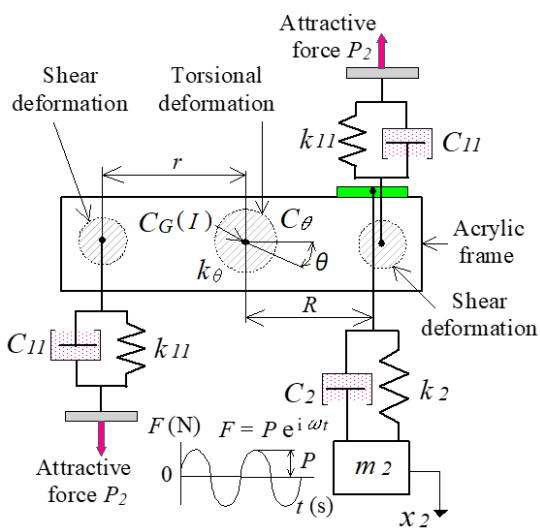

Fig. 4. Modeling of rotational movement.

As the analytical models for the above two types of actuator are identical, a vibration analysis is carried out using the two-degree-of-freedom model. The rubber sheet is treated as a linear spring. The mass of the permanent magnet in the vibration component is m_2, the spring constant of the coil spring is k_2, the mass of the actuator body (excluding mass m_2) is m_1, and the spring constant of the rubber sheet is k_1. The viscous damping coefficients of the rubber sheet and coil spring are C_1 and C_2, respectively. For the vibration analysis, the displacement coordinates of masses m_1 and m_2 are defined as x_1 and x_2, respectively. The coil spring is expressed in such a way that it can be used for both hard and soft springs. Nonlinearity is considered with respect to the displacement difference (x_2-x_1), as in equation (1). The equations of motion for the translational movement of the actuator subjected by an electromagnetic force to a forced harmonic excitation force $P\cos\omega t$ with force amplitude P and angular frequency ω, where t is time, are expressed for masses m_1 and m_2 as follows.

$$\left.\begin{aligned} m_1\frac{d^2x_1}{dt^2} &= -k_1x_1+\left[k_2\left(x_2-x_1\right)+\lambda\left(x_2-x_1\right)^3\right]-C_1\frac{dx_1}{dt}+C_2\left(\frac{dx_2}{dt}-\frac{dx_1}{dt}\right) \\ m_2\frac{d^2x_2}{dt^2} &= -\left[k_2\left(x_2-x_1\right)+\lambda\left(x_2-x_1\right)^3\right]-C_2\left(\frac{dx_2}{dt}-\frac{dx_1}{dt}\right)+P\cos\omega t \end{aligned}\right\} \tag{2}$$

Considering the stiffness and length of both the sheet and the spring, $x_2 >> x_1$. The restoring force $F(x)$ in the brackets is assumed to be approximately as follows.

$$F(x)=k_2\left(x_2-x_1\right)+\lambda\left(x_2-x_1\right)^3\cong k_2\left(x_2-x_1\right)+\lambda x_2^3=\left(k_2x_2+\lambda x_2^3\right)-k_2x_1 \tag{3}$$

For equation (3), consider a nonlinear restoring force F_2 (= $k_2x_2+\lambda x_2^3$) on a displacement x_2 of mass m_2. The displacements x_1 and x_2 are considered to vibrate harmonically under a forced harmonic excitation force. As B is the vibration amplitude and φ is the phase, the displacement x_2 is assumed to be as follows.

$$x_2=B\cos\varphi\ ,\quad \varphi=\omega t-\phi \tag{4}$$

Assuming that the nonlinearity of vibration component is relatively small, if the nonlinear restoring force F_2 is expressed using a Fourier series with D as the coefficient, the following equation is obtained.

$$F_2\left(x\right)=k_2x_2+\lambda x_2^3=k_2B\cos\varphi+\lambda B^3\cos^3\varphi=D\cos\varphi \tag{5}$$

D can be calculated using the same method as that used to find the coefficients of the Fourier series as follows.

$$D=\frac{1}{\pi}\int_0^{2\pi}\left(k_2B\cos\varphi+\lambda B^3\cos^3\varphi\right)\cos\varphi\,d\varphi=k_2B+\frac{3}{4}\lambda B^3 \tag{6}$$

From the restoring force $F_2(x_2) = D\cos\varphi$, the following equation is obtained.

$$F_2\left(x\right)=D\frac{x_2}{B}=\left(k_2B+\frac{3}{4}\lambda B^3\right)\frac{x_2}{B}=k_2^*x_2\ ,\quad k_2^*=k_2\left(1+\frac{3}{4}\beta B^2\right)\ ,\quad \beta=\frac{\lambda}{k_2} \tag{7}$$

k_2^* in the above equation represents the equivalent linear spring constant. If we introduce $Pe^{i\omega t}$, where i is the imaginary unit, instead of the forced harmonic excitation force $P\cos\omega t$ mentioned above, the equation of motion can be expressed as follows.

$$m_1\frac{d^2x_1}{dt^2}=k_2^*x_2-\left(k_1+k_2\right)x_1-C_1\frac{dx_1}{dt}+C_2\left(\frac{dx_2}{dt}-\frac{dx_1}{dt}\right),\ m_2\frac{d^2x_2}{dt^2}=k_2x_1-k_2^*x_2-C_2\left(\frac{dx_2}{dt}-\frac{dx_1}{dt}\right)+Pe^{i\omega t} \tag{8}$$

We assume the following general solution to equation (9).

$$x_1 = A e^{\mathrm{i}\omega t} \quad , \quad x_2 = B e^{\mathrm{i}\omega t} \tag{9}$$

By substituting equation (9) into equation (8) and expressing the vibration amplitude B for mass m_2 in matrix form, the following equation is obtained.

$$B = \frac{\begin{vmatrix} k_1 + k_2 - m_1\omega^2 + \mathrm{i}\omega(C_1 + C_2), & 0 \\ -(k_2 + \mathrm{i}\omega C_2) & , \quad P \end{vmatrix}}{\Delta}, \ \Delta = \left\{k_1 + k_2 - m_1\omega^2 + \mathrm{i}\omega(C_1 + C_2)\right\} \times \left(k_2^* - m_2\omega^2 + \mathrm{i}\omega C_2\right) - \left(k_2 + \mathrm{i}\omega C_2\right)^2 \tag{10}$$

The following quantities and dimensionless quantities are introduced.

$$\delta_{st} = \frac{P}{k_2},\ p_a = \sqrt{\frac{k_1}{m_1}},\ p = \sqrt{\frac{k_2}{m_2}},\ \alpha = \frac{m_2}{m_1},\ \overline{\omega} = \frac{\omega}{p},\ \overline{p}_a = \frac{p_a}{p},\ \overline{B} = \frac{B}{\delta_{st}},\ \overline{\beta} = \beta\delta_{st}^2,\ \varsigma_1 = \frac{C_1}{2\sqrt{m_2 k_2}},\ \varsigma_2 = \frac{C_2}{2\sqrt{m_2 k_2}} \tag{11}$$

Furthermore, the equivalent linear spring constant is expressed as the following equation.

$$k_2^* = k_2\left(1 + \frac{3}{4}\beta B^2\right) = k_2\varepsilon,\ \ \varepsilon = \left(1 + \frac{3}{4}\overline{\beta}\,\overline{B}^2\right) \tag{12}$$

When calculated using equation (11), the vibration amplitude B for mass m_2 is expressed as follows.

$$B = \frac{\delta_{st}(a_5 + \mathrm{i}\,a_6)}{a_1 + a_2\varepsilon + \mathrm{i}(a_3 + a_4\varepsilon)} \tag{13}$$

where

$$\left.\begin{aligned} &a_1 = \overline{\omega}^2\left(\overline{\omega}^2 - \overline{p}_a^2 - \alpha - 4\alpha\varsigma_1\varsigma_2\right),\ a_2 = \overline{p}_a^2 - \overline{\omega}^2,\ a_3 = 2\varsigma_2\overline{\omega}\left(\overline{p}_a^2 - \overline{\omega}^2 - \alpha\overline{\omega}^2\right) - 2\alpha\varsigma_1\overline{\omega}^3,\ a_4 = 2\alpha\varsigma_1\overline{\omega} \\ &a_5 = \overline{p}_a^2 - \overline{\omega}^2 + \alpha\ ,\ \ a_6 = 2\alpha\overline{\omega}\left(\varsigma_1 + \varsigma_2\right) \end{aligned}\right\} \tag{14}$$

Equation (13) can be rewritten as the following equation.

$$B = B_b e^{\mathrm{i}(\phi_1 - \phi_2)},\ B_b = \frac{\delta_{st}\sqrt{a_5^2 + a_6^2}}{\sqrt{\left(a_1 + a_2\varepsilon\right)^2 + \left(a_3 + a_4\varepsilon\right)^2}},\ \ \tan\phi_1 = \frac{a_6}{a_5},\ \ \tan\phi_2 = \frac{a_3 + a_4\varepsilon}{a_1 + a_2\varepsilon} \tag{15}$$

B_b in the above equation is the actual vibration amplitude for mass m_2, so amplitude B is replaced with B_b. Furthermore, by introducing the dimensionless vibration amplitude $\overline{B}_b\left(= B_b/\delta_{st}\right)$ and expanding B_b in equation (15), the following sixth-order equation is derived.

$$\frac{9}{16}\eta_1\overline{\beta}^2\overline{B}_b^6 + \frac{3}{2}\eta_2\overline{\beta}\overline{B}_b^4 + \eta_3\overline{B}_b^2 - \eta_4 = 0 \tag{16}$$

where

$$\eta_1 = a_2^2 + a_4^2,\ \eta_2 = a_2^2 + a_4^2 + a_1a_2 + a_3a_4,\ \eta_3 = a_1^2 + a_2^2 + a_3^2 + a_4^2 + 2a_1a_2 + 2a_3a_4,\ \eta_4 = a_5^2 + a_6^2 \tag{17}$$

The real root of equation (16) represents the dimensionless vibration amplitude for mass m_2. The dimensionless vibration amplitudes were calculated using a MATLAB program.

4. Vibration analysis for rotational movement

The case of two vibration components (A and C) operating is discussed next. When vibration component C vibrates as shown in Figures 1 and 4, it is assumed that the main part of the three rubber sheets attached to the support deforms in torsion and that the two secondary-parts deform in shear. Let I be the moment of inertia around the center of gravity of the actuator. Let k_θ and C_θ be the spring constant and viscous damping coefficient of the torsional deformation, respectively, of the rubber sheet attached to the main permanent magnet. Let k_{11} and C_{11} be the spring constant and viscous damping coefficient of shear deformation, respectively, of the rubber sheet attached to the secondary-permanent magnet. Let x_2 be the displacement coordinate of mass m_2 and θ be the rotation coordinate around the center of gravity C_G of the actuator. In this actuator, the center of vibration component A is the center of gravity C_G. When the actuator is subjected to forced excitation force $Pe^{i\omega t}$, considering the nonlinearity regarding the displacement difference (x_2-$R\theta$), the equations of translational movement for mass m_2 and the equation of rotational movement around the center of gravity C_G, with moment of inertia I, are expressed respectively as follows.

$$\left.\begin{aligned} m_2\frac{d^2x_2}{dt^2} &= -\left[k_2(x_2-R\theta)+\lambda(x_2-R\theta)^3\right]-C_2\left(\frac{dx_2}{dt}-R\frac{d\theta}{dt}\right)+Pe^{i\omega t} \\ I\frac{d^2\theta}{dt^2} &= \left[k_2(x_2-R\theta)+\lambda(x_2-R\theta)^3\right]R-2rk_{11}(r\theta)-k_\theta\theta-2C_{11}\left(r\frac{d\theta}{dt}\right)r+C_2\left(\frac{dx_2}{dt}-R\frac{d\theta}{dt}\right)R-C_\theta\frac{d\theta}{dt} \end{aligned}\right\} \tag{18}$$

Similar to equation (3), the restoring force $F(x)$ within the brackets is assumed to be as follows.

$$F(x)=k_2(x_2-R\theta)+\lambda(x_2-R\theta)^3 \cong k_2(x_2-R\theta)+\lambda x_2^3=(k_2x_2+\lambda x_2^3)-k_2R\theta \tag{19}$$

In equation (18), the nonlinear restoring force F_2 (= $k_2x_2+\lambda x_2^3$) with respect to displacement x_2 is analyzed using the Fourier series, as in the case of translational movement. Using the equivalent linear spring constant k_2^* in equation (7), the equation of motion (18) can be expressed as follows.

$$\left.\begin{aligned} m_2\frac{d^2x_2}{dt^2} &= -k_2^*x_2+k_2R\theta-C_2\left(\frac{dx_2}{dt}-R\frac{d\theta}{dt}\right)+Pe^{i\omega t} \\ I\frac{d^2\theta}{dt^2} &= (k_2^*x_2-k_2R\theta)R-k_\theta\theta-2rk_{11}(r\theta)-2C_{11}\left(r\frac{d\theta}{dt}\right)r+C_2\left(\frac{dx_2}{dt}-R\frac{d\theta}{dt}\right)R-C_\theta\frac{d\theta}{dt} \end{aligned}\right\} \tag{20}$$

Due to the small vibration amplitude, the following equation was assumed.

$$x_1=R\theta \ , \ \frac{dx_1}{dt}=R\frac{d\theta}{dt} \ , \ \frac{d^2x_1}{dt^2}=R\frac{d^2\theta}{dt^2} \tag{21}$$

We assume the following general solution to the equation of motion.

$$x_1=R\theta=R\vartheta e^{i\omega t}=Ae^{i\omega t} \ , \quad x_2=Be^{i\omega t} \tag{22}$$

Now substitute equation (22) into equation (20) and introduce equation (11) and the following various quantities and dimensionless quantities.

$$\bar{I}=\frac{I}{m_1R^2}, \ \bar{r}=\frac{r}{R}, \ p_r=\sqrt{\frac{k_r}{m_1}}=\sqrt{\frac{k_{11}+(k_\theta/2r^2)}{m_1}} \ , \quad \bar{p}_r=\frac{p_r}{p}, \ \varsigma_r=\frac{C_r}{2\sqrt{m_2k_2}}=\frac{1}{2\sqrt{m_2k_2}}\left(C_{11}+\frac{C_\theta}{2r^2}\right) \tag{23}$$

If the calculations are performed as in the case of translational movement, the following sixth-order equation regarding the dimensionless vibration amplitude $\bar{B}_b(=B_b/\delta_{st})$ is derived.

$$\left.\begin{aligned}&\frac{9}{16}\sigma_1\bar{\beta}^2\bar{B}_b^6+\frac{3}{2}\sigma_2\bar{\beta}\bar{B}_b^4+\sigma_3\bar{B}_b^2-\sigma_4=0\\&\sigma_1=b_2^2+b_4^2,\ \sigma_2=b_2^2+b_4^2+b_1b_2+b_3b_4,\ \sigma_3=b_1^2+b_2^2+b_3^2+b_4^2+2b_1b_2+2b_3b_4,\ \sigma_4=b_5^2+b_6^2\end{aligned}\right\} \tag{24}$$

where

$$\left.\begin{aligned}&b_1=\bar{\omega}^2\left(\bar{I}\bar{\omega}^2-2\bar{r}^2\bar{p}_r^2-\alpha-8\bar{r}^2\alpha\varsigma_r\varsigma_2\right),\ b_2=2\bar{r}^2\bar{p}_r^2-\bar{I}\bar{\omega}^2,\ b_4=4\bar{r}^2\alpha\varsigma_r\bar{\omega}\\&b_3=2\varsigma_2\bar{\omega}\left(2\bar{r}^2\bar{p}_r^2-\bar{I}\bar{\omega}^2-\alpha\bar{\omega}^2\right)-4\bar{r}^2\alpha\varsigma_r\bar{\omega}^3,\ b_5=2\bar{r}^2\bar{p}_r^2-\bar{I}\bar{\omega}^2+\alpha,\ b_6=2\alpha\bar{\omega}\left(\varsigma_2+2\bar{r}^2\varsigma_r\right)\end{aligned}\right\} \tag{25}$$

5. Static analysis for translational movement of phase-controlled actuator

It is assumed that the vibration amplitude for mass m_1 can be omitted because it is smaller than the vibration amplitude for mass m_2, as shown in equations (3) and (19). For the vibration amplitude B_b obtained from the vibration analysis, the amplitudes and generated forces obtained when vibration components A, B and C vibrate are respectively defined as B_{be} and F_A, B_{bs} and F_B, and B_{br} and F_C, respectively. The vibration amplitudes calculated by the vibration analysis described above are assumed to move linearly and rotationally while maintaining a steady state. In a previous paper [10], the basis of the energy balance method was established, and the calculated values were in good agreement with the experimental values. In this method, when vibration component A is displaced with amplitude B_{be} in the $+z$ direction (minimum attraction force), the maximum elastic energy U in vibration component B or C is equal to the dissipated energy due to friction and the work done by gravity. By using this energy method presented by the authors [10], the effects of the load mass and traction force were incorporated and a static analysis of the actuator's movement was performed.

Figure 5 shows a situation in which an actuator is held on a sloped magnetic material with angle η by the attractive force of the permanent magnet. Figure 5(a) shows the case where vibration components A and B vibrate in the $+z$ and $-x$ coordinate directions and generate forces F_A and F_B, respectively. Let m be the total mass of the actuator, M be the load mass acting on the center of gravity, and W be the traction force. If μ is the dynamic friction coefficient, the following equation can be obtained from the friction force F_f when the actuator moves along the slope moves along the slope (climbing) and the balance of forces along the slope, where g is the gravitational acceleration.

$$F_f=\mu\left[(m+M)\,g\cos\eta+P_1+2P_2-F_A\right],\ F_B=F_f+(m+M)\,g\sin\eta+W \tag{26}$$

Figure 5(b) shows the case where vibration components A and B vibrate in the $-z$ and $+x$ coordinate directions. The following equation can be obtained from the balance between the frictional force F_b in the case of backward movement (downhill) and the force on the slope.

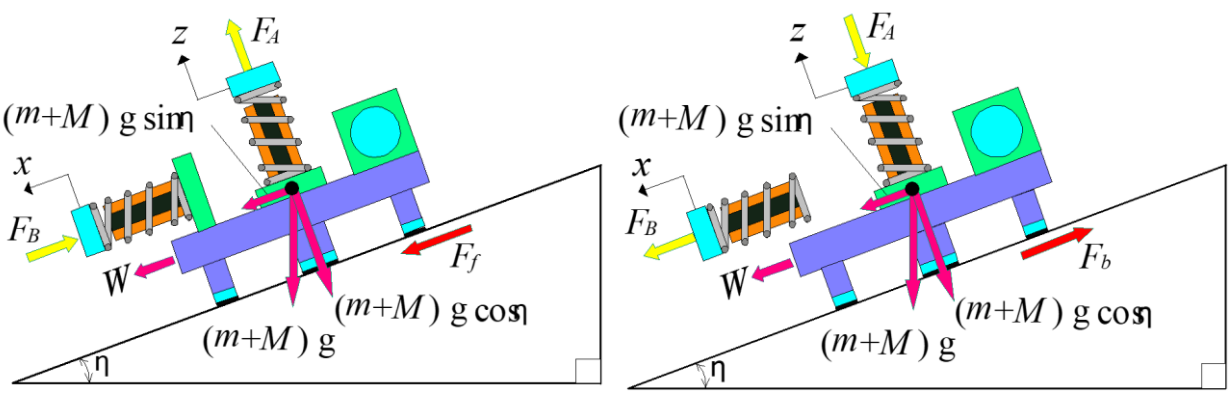

(a) Balance of forward (b) Balance of backward

Fig. 5. Actuator moving on slope with angle η.

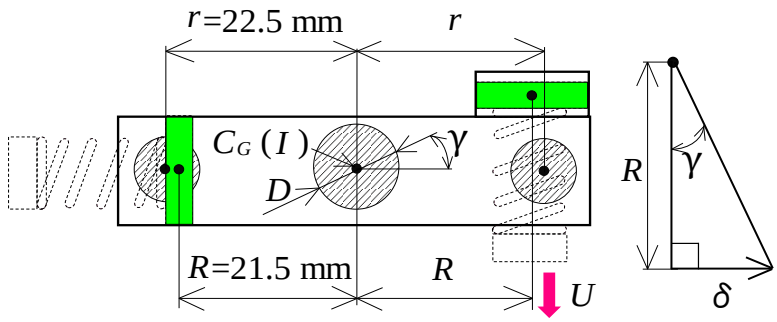

Fig. 6. Actuator specifications for rotational movement.

$$F_b = \mu\left[(m+M)\,g\cos\eta + P_1 + 2P_2 + F_A\right]\ ,\ F_B = F_b - (m+M)\,g\sin\eta - W \tag{27}$$

As $F_A = k_2 \times B_{be}$ in the above equations, the following dimensionless quantities and quantities U are introduced.

$$\overline{F}_A = \frac{F_A}{P_1},\ \overline{P}_2 = \frac{P_2}{P_1},\ \overline{m} = \frac{mg}{P_1},\ \overline{M} = \frac{Mg}{P_1}\ ,\ \overline{M}_m = \overline{M} + \overline{m}\ ,\ \overline{W} = \frac{W}{P_1},\ \overline{U} = \frac{U}{P_1},\ U = \frac{1}{2}\,k_2\,B_{bs}^2 \tag{28}$$

Let τ be the phase difference in displacement between vibration components A and B. By equating the elastic energy U of vibration component B when it vibrates with amplitude B_{bs} with the dissipated energy $F_f\,\delta_f$ and $F_b\,\delta_b$ due to frictional forces and the work done by gravity, the forward and backward displacements can be respectively expressed as follows.

$$\delta_f = \frac{\overline{U}\cos\tau}{\mu\left\{\overline{M}_m\cos\eta + 1 + 2\overline{P}_2 - \overline{F}_A\right\} + \overline{M}_m\sin\eta + \overline{W}}\quad ,\quad \delta_b = \frac{\overline{U}\cos\tau}{\mu\left\{\overline{M}_m\cos\eta + 1 + 2\overline{P}_2 + \overline{F}_A\right\} - \overline{M}_m\sin\eta - \overline{W}} \tag{29}$$

If the driving frequency of the vibration component is f (Hz), the translational speed of the actuator v_{lin} can be found as follows.

$$v_{lin} = f\left(\delta_f - \delta_b\right) \tag{30}$$

6. Static analysis for rotational movement of phase-controlled actuator

Figure 6 shows the state in which the actuator is held on a horizontal plane. A permanent magnet with attractive force P_2 is installed at position r from the center of gravity C_G of the actuator and vibration component C is installed at position R. Let Q be the total force acting on the main permanent magnet. The moment N due to the frictional force when the main permanent magnet with radius D rotates around the center of gravity C_G is expressed as follows [17].

$$N = \frac{2}{3}\mu Q D\ ,\quad Q = mg + Mg + P_1 \tag{31}$$

As shown in Figure 2(b), when vibration component A vibrates in the $+z$ coordinate direction with amplitude B_{be}, the generated force acting on the actuator support is F_A ($= k_2 \times B_{be}$). The moment M_f due to the frictional force around the actuator center of gravity C_G is expressed as follows.

$$M_f = 2\mu P_2 r + \frac{2}{3}\mu\left(mg + Mg + P_1 - F_A\right)D \tag{32}$$

When vibration component A vibrates in the $-z$ coordinate direction with amplitude B_{be}, the moment M_b due to the frictional force around the actuator center of gravity C_G is as follows.

$$M_b = 2\mu P_2 r + \frac{2}{3}\mu\left(mg + Mg + P_1 + F_A\right) D \tag{33}$$

The total area of the permanent magnet is S (= S_1 + 2S_2) and the loads acting on the main permanent magnet with area S_1 and the secondary-permanent magnet with area S_2 are distributed based on the area ratio. Furthermore, equation (28) and the following dimensionless quantities are used for the elastic energy U of vibration component C when it vibrates with amplitude B_{br}.

$$\overline{S}_1 = \frac{S_1}{S},\ \overline{S}_2 = \frac{S_2}{S},\ \overline{r} = \frac{r}{R},\ \overline{D} = \frac{D}{R},\ U = \frac{1}{2}k_2 B_{br}^2 \tag{34}$$

The elastic energy U and the moment dissipation energies $M_f\delta_f$ and $M_b\delta_b$ due to frictional forces are equated. If the phase difference in displacement between vibration components A and C is τ, the forward and backward angular displacements can be expressed as follows.

$$\delta_f = \frac{\overline{U}\cos\tau}{2\mu\xi_1\overline{r} + \frac{2}{3}\mu\xi_2\overline{D}},\ \delta_b = \frac{\overline{U}\cos\tau}{2\mu\xi_3\overline{r} + \frac{2}{3}\mu\xi_4\overline{D}} \tag{35}$$

where

$$\xi_1 = \overline{P}_2 + \overline{S}_2\left(\overline{M}_m - \overline{F}_A\right),\ \xi_2 = 1 + \overline{S}_1\left(\overline{M}_m - \overline{F}_A\right),\ \ \xi_3 = \overline{P}_2 + \overline{S}_2\left(\overline{M}_m + \overline{F}_A\right),\ \xi_4 = 1 + \overline{S}_1\left(\overline{M}_m + \overline{F}_A\right) \tag{36}$$

From this, the amount of movement δ during one cycle of vibration is as follows.

$$\delta = \delta_f - \delta_b \tag{37}$$

Referring to Figure 6, as f (Hz) is the driving frequency, the rotation angle γ in one cycle of vibration and the rotation speed per second v_{rot} are expressed as follows.

$$v_{rot} = f\theta,\ \tan\gamma = \frac{\delta}{R},\ \gamma = \tan^{-1}\left(\frac{\delta}{R}\right) \tag{38}$$

The mounting positions of vibration components B and C are equal from the frame center of gravity C_G. Therefore, if the actuator is installed on a vertical plane, the moments due to the gravity of the components cancel each other, so the results of this analysis can also be applied to a vertical plane.

7. Parameters for numerical calculations

7.1. Parameters of actuator for numerical calculations

In numerical calculations, as parameters of the actuator, the mass of the permanent magnet in the vibration component was m_2 = 0.0043 kg and the mass of the actuator body was m_1 = 0.052 kg. The linear spring constant of the coil spring was k_2 = 1,836 N/m and the nonlinear coefficient in equations (7) and (12) was β = -0.0155 for a soft spring. Using the force gage, the attractive force in the main permanent magnet to which the rubber sheet was attached was P_1 = 1.72 N and the attractive force in the secondary-permanent magnet was P_2 = 0.93 N. The dynamic friction coefficient between the rubber sheet and the surface plate was μ = 0.84. The modulus of elasticity of natural rubber sheet is $E = 6.9552\times10^5$ N/m^2. In addition, the mass and dimensions of each part of the actuator were measured. Using the parallel axis theorem, the moment of inertia around the actuator center of gravity C_G was calculated to be $I = 3.48\times10^{-5}$ kgm^2.

7.2. Forced harmonic excitation force

By combining a force gauge and an x-y stage, the relationship between the DC input to the electromagnet in the vibration component and the force generated in the permanent magnet was measured. The measurement results are shown in Figure 7. In this actuator, the input current to the electromagnet was limited to 150 mA in consideration of

heat generation. From this, the relationship between the DC current I_{in} (A) and the average value P (N) of the attractive and repulsive forces can be expressed by the following equation.

$$P\,(\mathrm{N}) = 1.667\, I_m\,(\mathrm{A}) - 0.001155 \tag{39}$$

When the actuator was driven, the effective (root-mean-square, RMS) value I_m of the AC current input to the electromagnet in the vibration component was measured by a power analyzer. The force amplitude P (N) of the forced harmonic excitation force shown in equations (8) and (18) was determined as 1.41 times the P (N) value calculated using equation (39).

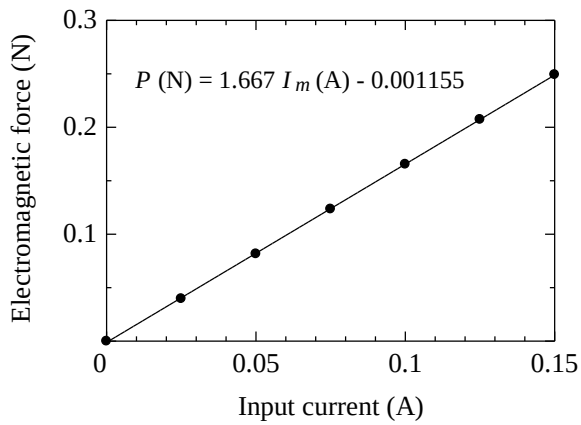

Fig. 7. Relationship between input current to electromagnet and electromagnetic force.

7.3. Spring constants of natural rubber sheet

Assuming that the thickness of the rubber sheet is h and the diameters of the main part and secondary parts are D (area S_1) and d (area S_2), respectively, the spring constant k_1 in the case of the compression-tension deformation of three rubber sheets can be calculated using equation (40).

$$k_1 = \frac{ES}{h},\ S = \left(S_1 + 2S_2\right) \tag{40}$$

On the other hand, taking G as the transverse modulus of elasticity and Poisson's ratio as $\nu = 0.5$, the spring constant k_1 for the shear deformation of the three rubber sheets and the spring constant k_{11} for the shear deformation of one rubber sheet in the secondary magnet can be calculated.

$$k_1 = \frac{GS}{h},\ k_{11} = \frac{GS_2}{h},\ G = \frac{E}{2\left(1+\nu\right)} \tag{41}$$

Furthermore, with I_p as the second moment of the section, the spring constant k_θ in the torsional deformation of the rubber sheet in the main magnet can be calculated using equation (42).

$$k_\theta = \frac{GI_p}{h},\quad I_p = \frac{\pi D^4}{32} \tag{42}$$

7.4. Damping of coil spring and natural rubber sheet

A one-degree-of-freedom model was fabricated by attaching a 50-g mass to a rubber sheet with a thickness of 3 mm and a diameter of 7 mm. The logarithmic damping coefficient δ_d was measured by shearing and torsionally deforming the rubber sheet. The viscous damping coefficients C_{11} and C_θ were then calculated. When the rubber sheet expands and contracts, the spring constant is very high, so the damping during expansion and contraction was ignored. For the coil spring, the viscous damping coefficient $C_2 = 0.0815$ Ns/m was determined due to the compression and tension vibration of the vibration component.

The spring constant and viscous damping coefficient during translational and rotational movement of the rubber sheet are shown in Tables 1 and 2, respectively.

Table 1: Spring constant and viscous damping coefficient for translational movement.

Compression-tension deformation		**Shear deformation**	
k_1 (N/m)	1.245×10^{7}	k_1 (N/m)	4.15×10^{4}
C_1 (Ns/m)	0	C_1 (Ns/m)	1.937

Table 2: Spring constant and viscous damping coefficient for rotational movement.

Torsional deformation		**Shear deformation**	
k_θ (N/m)	0.226	k_{11} (N/m)	1.165×10^{4}
C_θ (Ns/m)	1.91×10^{-4}	C_{11} (Ns/m)	1.937

8. Frequency response of phase-controlled actuator

In Experiment, an iron surface plate (300 mm wide, 300 mm long, and 60 mm thick) was used as the magnetic material. The phase-controlled actuator was mounted on the surface plate and the actuator was driven by two two-channel signal generators and three amplifiers. The input current and power to the electromagnets of the vibration components were measured using a three-channel power analyzer. Each vibration component was excited by a sinusoidal wave. Two two-channel signal generators were used to adjust the phase to the vibrations in each vibration component using a phase adjustment function. The phase-controlled actuator was set on a horizontal plane and the vibration amplitudes of the vibration components were measured during movement using a laser displacement meter and a high-speed data logger, as shown in Figure 8. For translational and rotational movement, laser displacement meters were placed at the moving points of the actuator, as shown in Figures 8(a) and 8(b). The movement speed was simultaneously measured.

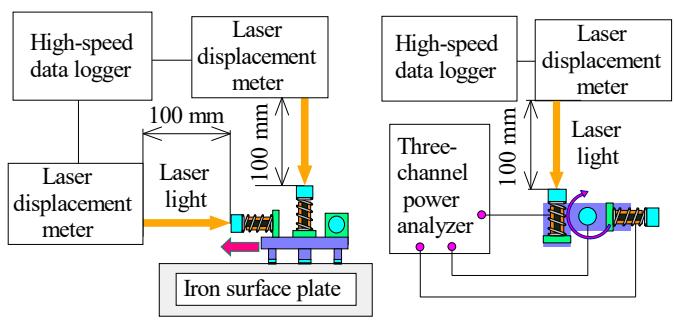

(a) Translational movement (b) Rotational movement

Fig. 8. Experimental apparatus.

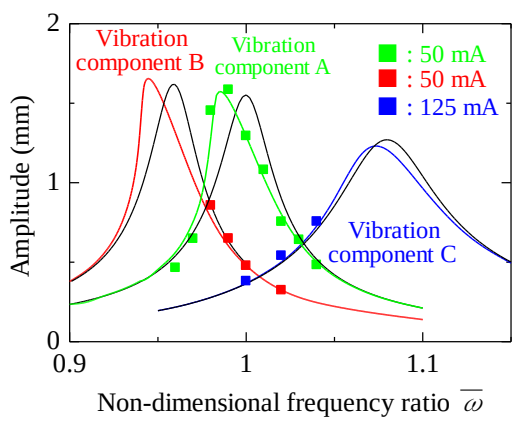

Fig. 9. Frequency response of each vibration component.

Figure 9 shows the relationship between the vibration amplitude of each vibration component and the vibration frequency ratio F_r normalized by the resonance frequency 104 Hz (linear) for vibration component A at small amplitudes. As mentioned, the actuator performs a translational movement when vibration components A and B are driven and a rotational movement when vibration components A and C are driven. In this figure, the measurement results obtained when 50- and 125-mA current (RMS values) was input to the electromagnets are shown. The green line shows the results of the nonlinear theoretical analysis when vibration component A is driven, and the red and blue lines show the results of the nonlinear theoretical analysis when vibration components B and C are driven. The black solid line shows the results of the analysis in the linear case. It can be observed that the displacement response is influenced by the soft springs. The response curves calculated with the nonlinearity of the springs taken into account are in good agreement with the experimentally measured results.

The frequency response was measured in preliminary experiments by fixing the actuator with various adhesives and adhesive tapes. However, because the rubber sheet in this actuator is only 1 mm thick, the various adhesives caused considerable variation in the measured values. Therefore, the frequency response of the actuator while it was moving was measured experimentally. The measurement results showed that the vibration displacement of vibration component remained in a steady state while the actuator was moving. From Figure 9, the measurement and calculation results show that the resonance frequencies of vibration components A, B or C are quite different. In this actuator, the change in the attraction force due to the vibration displacement of vibration component A has a significant effect on the movement characteristics of the actuator. It is necessary to drive vibration components B and C near the resonance frequency of vibration component A, which is the basis of the operation of this actuator. The frequency response near the resonance frequencies of vibration components B and C could not be measured due to reasons that prevented the actuator from movement. In the future, based on the theoretical analysis obtained in this paper, the actuator should be designed so that the resonance frequencies of vibration components A, B, and C can be tuned.

9. Movement characteristics of phase-controlled actuator

Each vibration component was driven at 104 Hz, the resonant frequency at small amplitude in vibration component A. At first, the translational and rotational movement of the actuator was considered with the load mass M and traction force W set to zero.

The prototype actuator was placed in the horizontal plane and vibration component A and vibration component B or C were driven. Tables 3 and 4 show the translational and rotational speeds when the input current to vibration component A was fixed at 50 mA and the input current I_{in} to vibration components B or C was varied. The directions of translation and rotation in Tables 3 and 4 correspond to the directions shown in Figures 2(a) and 2(b). In this case, the phase difference of vibration between vibration components A and B or C was adjusted to 0 (in phase) and 180 (out of phase) degrees. The tables also show the results calculated by theoretical analysis. This actuator is capable of translational and rotational reciprocation at approximately the same speed.

Figure 10 shows the relationship between the input current I_{in} to vibration component B and the translation speed v_{lin} for horizontal and vertical planes, with the input current to the vibration component A set to 50 and 75 mA (RMS values). In the figure, empty and filled symbols are the measurement results for the horizontal and vertical planes, respectively. The black dashed and solid lines are the results of the analyses for the horizontal and vertical planes, respectively, calculated using equations (16) and (30). The red solid line shows the linear analysis results for the horizontal plane obtained when the input current to vibration component A was 50 mA. As the input current to the electromagnet is increased and the vibration amplitude of vibration component is increased, the difference between the nonlinear and linear analysis results increases.

Figure 11 shows the relationship between the input current I_{in} to component C and the rotational speed v_{rot} in the clockwise direction obtained when the input current to vibration component A was 25, 50, and 75 mA (RMS values). Empty and filled symbols show the results for the horizontal and vertical planes, respectively. The black solid lines show the nonlinear analysis results calculated using equations (24) and (38). The red solid line shows the linear analysis results obtained when the input current to vibration component A was 50 mA. The figures show that the rotational speeds in the horizontal and vertical planes are almost identical.

The load characteristics of the actuator are discussed next. The load mass was attached to the main permanent magnet of the actuator using a string. Figure 12 shows the relationship between the load mass M on the actuator and the

vertical upward speed v_{up}, with the input current I_{in} to vibration component A fixed at 75 mA and the input current to component B varied. The filled circles, triangles, and squares show the measurement results obtained when the input current to vibration component B was 150, 100 and 75 mA, respectively.

Table 3: Relationship between input current and translational speed.

Input current I_{in} to vibration component B (mA)	**x direction (in phase)**		**-x direction (out of phase)**	
	Measured value v_{lin} (mm/s)	Calculated value v_{lin} (mm/s)	Measured value v_{lin} (mm/s)	Calculated value v_{lin} (mm/s)
50	10.89	11.01	10.72	11.01
75	23.11	22.7	22.76	22.7

Table 4: Relationship between input current and rotational speed.

Input current Iin to vibration component C (mA)	**Clockwise (in phase)**		**Counterclockwise (out of phase)**	
	Measured value v_{rot} (degrees/s)	Calculated value v_{rot} (degrees/s)	Measured value v_{rot} (degrees/s)	Calculated value v_{rot} (degrees/s)
75	10.71	10.41	10.03	10.41
100	18.82	18.29	18.48	18.29

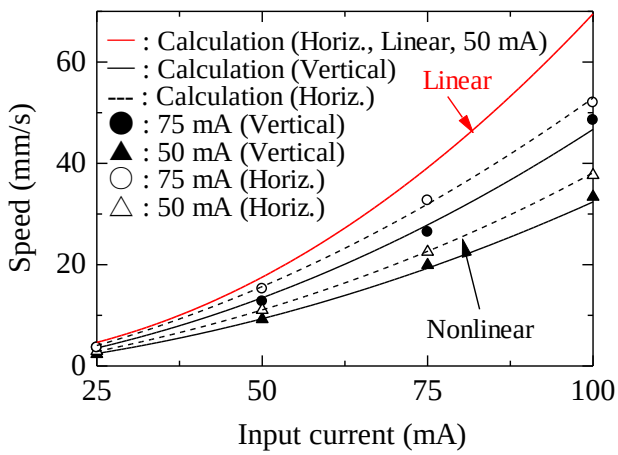

Fig. 10. Relationship between input current and translational speed (filled symbols: vertical plane, empty symbols: horizontal plane)

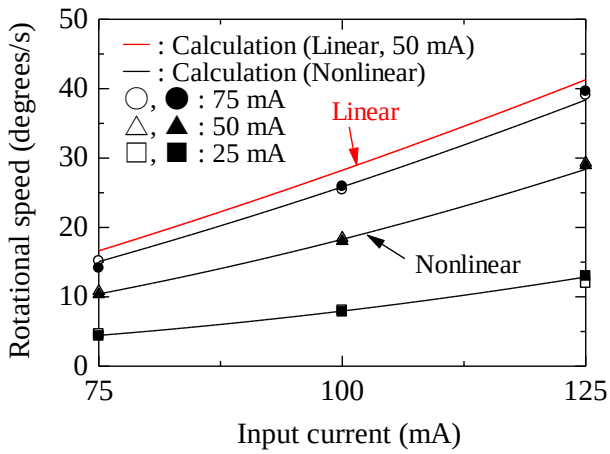

Fig. 11. Relationship between input current and rotational speed (filled symbols: vertical plane, empty symbols: horizontal plane).

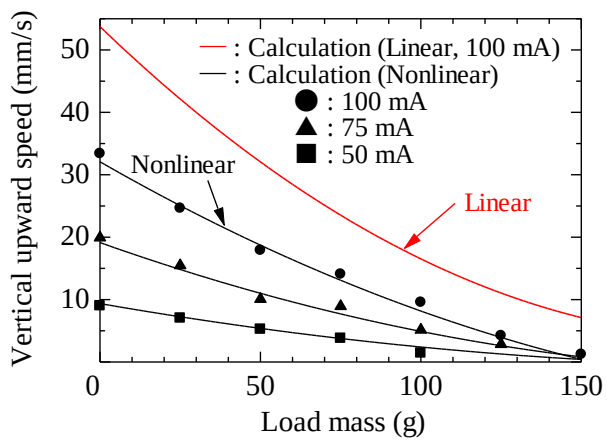

Fig. 12. Relationship between load mass and vertical upward speed.

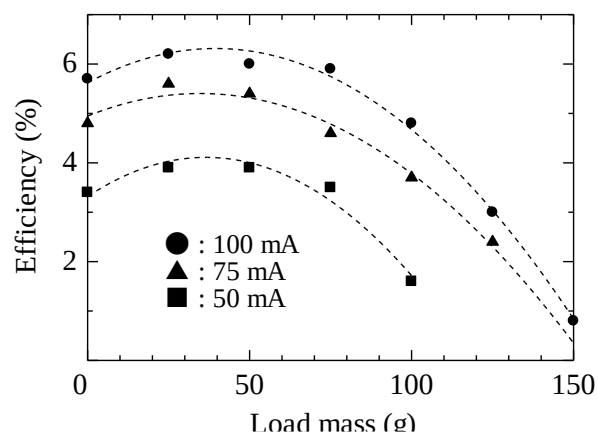

Fig. 13. Relationship between load mass and efficiency.

The black solid lines are the calculation results calculated using equation (30) with $\eta = 90°$. The red solid line shows the results of a linear analysis obtained when the input current to vibration component B was 100 mA. The figure shows that the phase-controlled actuator is capable of pulling an additional mass of 150 g. One of the applications of this phase-controlled actuator is to be equipped with an inspection system. To mount the inspection system on the actuator, the acrylic frame shown in Figure 1 is extended. A small camera (mass: 10 g) with a built-in transmitter and a battery (mass: 42 g) can be mounted on this part to inspect iron structures.

Figure 13 shows the relationship between the load mass and self-propelled efficiency of the actuator when the input current I_{in} to vibration component A is fixed at 50 mA and the input current to vibration component B is varied. The efficiency e_f is expressed as follows.

$$e_f\,[\%] = (m + M)\, v_{up}\, g \times 100 \,/\, P_I \tag{43}$$

where m (= m_1 + m_2) is the total mass of the actuator, M is the load mass, g is the acceleration of gravity, and P_I is the input power. In the figure, the dashed lines show the quadratic approximation of the measured values obtained using the least-squares method. From the figure, the maximum efficiency of the actuator is approximately 6.2%.

Considering the above results, for actuators that can move by excitation of the vibration component, there are many combinations of magnetic circuits and vibration components in the excitation section. Even if the above combinations vary, the propulsion and the movement characteristics of the actuator can be predicted by calculation by measuring the excitation force by electromagnetic force, spring constants, and nonlinear coefficients. Therefore, the results obtained from this theoretical analysis can be used to design actuators according to various driving conditions and then build a prototype of the actual machine.

10. Conclusion

In this study, a new phase-controlled actuator capable of both translational and rotational motion has been proposed. In addition, a vibration analysis considering the nonlinearity of the coil spring in the vibration component and a static analysis of the movement of the phase-controlled actuator were carried out. An actual prototype of the phase-controlled actuator was built and its movement characteristics were measured. The results of the theoretical analysis well agreed with the measurement results, verifying the validity of the theoretical analysis. Tests on the actual device confirmed that the speed and direction in translation and rotation could be controlled with an error of less than approximately 3.7% when the phase difference of the vibration was set to 0 (in phase) or 180 (out of phase) degrees.

The operating principle and theoretical analysis method of the phase-controlled actuator, which is lightweight, compact and has good drivability, were established. It was shown that the movement characteristics can be predicted using only calculation. The equivalent linearization method presented in this paper has a clear theoretical analysis and can be extended to other nonlinear models in models with weak nonlinearities. The potential application of this actuator as a drive source for work or inspection robots was demonstrated in this paper.

Acknowledgement

This work was supported by JSPS KAKENHI Grant Number JP23K03648.

References

[1] Park J, Noh S. Task planning of transfer robots using reinforcement learning. IFIP Int Conf Adv Prod Manag Syst. 2023;591–602.
[2] Itoh T, Hosaka K, Nishimura K. Development of automatic reinforcing bar binding robot. JSME ROBOMECH. 2017;1–4.
[3] Jiang Y, Han Q, Dai Z, Zhou C. Structural design and kinematic analysis of a welding robot for liquefied natural gas membrane tank automatic welding. Int J Adv Manuf Technol. 2022;122:461–474.
[4] Ito M, Naganawa A. Method for low-speed driving of a standing-wave-type ultrasonic actuator. Trans JSME (in Japanese). 2011;77(775):519–523.

[5] Morita T, Kuribayashi M, Higuchi T. A cylindrical micro ultrasonic motor using PZT thin film deposited by single process hydrothermal method. IEEE Trans Ultrason. 1998;45(5):1178–1187.
[6] Takemura K, Maeno T. Design and control of an ultrasonic motor capable of generating multi-DOF motion. IEEE/ASME Trans Mechatronics. 2001;6(4):499–506.
[7] Takemura K, Maeno T. Development of a master-slave system for active endoscope using a multi-DOF ultrasonic motor. Trans Control Autom Syst Eng. 2002;4(1):17–22.
[8] Tsukakoshi M, Matsuse K. Analysis of phase control characteristics for vector control of wound-field synchronous motor at a modulation ratio. IEEJ Trans Ind Appl. 2010;131(9):1149–1156.
[9] Ogawa H, Ono M, Ban N, Ishida Y. Two stage control of a DC motor using an optimal control scheme. Trans Soc Instrum Control Eng. 2010;9(17):120–126.
[10] Yaguchi H, Sato R. A new type of electromagnetic vibration actuator capable of combined linear and rotational motion. Int J GEOMATE. 2024;26(117):68–77.
[11] Yaguchi H, Yamori S. Magnetic actuator capable of in-plane movement by phase control of vibration components. IEEE Trans Magn. 2022;58(8):1–6.
[12] Takahashi K, Fujimato K, Muranaka K, Tagawa K. An analysis of nonlinear vibrations of cables by harmonic balance method. J Jpn Soc Civ Eng. 1983;338(10):59–68.
[13] Okabe T, Kondo T. Improvement to the averaging method using the Jacobian elliptic function. J Sound Vib. 2009;320(2):339–364.
[14] Zhiqiang H, Xun P, Gang L, Lei H. Response of a two-degree-of-freedom vibration system with rough contact interfaces. Shock Vib. 2019;2019(1):1–13.
[15] Mahmoud B, Monique H, Livija C, Paul Z. Nonlinear analysis of two-degree of freedom system with nonlinear springs. Mech Syst Signal Process. 2022;171(15):1–11.
[16] Yaguchi H, Sato R. Nonlinear motion analysis of new electromagnetic vibration actuator. J Res Appl Mech Eng. 2024;12(2):1–10.
[17] Aoki H, Kitani S. Industrial mechanics. 4th ed. Japan: Morihoku Company; (in Japanese).